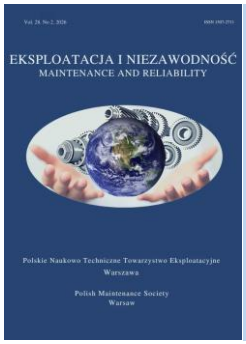

Eksploatacja i Niezawodnosc – Maintenance and Reliability
Volume 28 (2026), Issue 2
journal homepage: http://www.ein.org.pl

Article citation info:
Liu X, Sun C, Li T, Aero-engine remaining useful life prediction: An adaptive method for individual differences of engines, Eksploatacja i Niezawodnosc – Maintenance and Reliability 2026: 28(2) http:/10.17531/ein/214135

Aero-engine remaining useful life prediction: An adaptive method for individual differences of engines

Indexed by:
Web of Science Group

Xingchen Liu[a,*], Chenfeng Sun[a], Tianyu Li[a]

[a] Naval Aviation University, China

Highlights

- The method fully considers the influence of individual differences among engines.
- The proposed model has high prediction accuracy and good generalization.
- The method has higher accuracy and better robustness compared with other methods.

Abstract

The remaining useful life (RUL) prediction of aero-engine is of great significance for flight safety. The existing methods do not fully consider the influence of the individual differences of engines on the degradation process. And these methods are difficult to extract key features in highly coupled data, resulting in low prediction accuracy. To solve the problems, an adaptive prediction method for individual differences of engines is proposed. Firstly, the position of the First Prediction Time (FPT) is determined by calculating the maximum volatility value of the Health Indicator (HI) curve, so as to obtain the accurate RUL label. On this basis, the improved Temporal Convolutional Network (TCN) model is used to capture both local degradation patterns and global features. Then enter the bidirectional cyclic network to model the temporal features in the forward and backward directions. Finally, the accurate RUL value is obtained through the deep regression network. Compared with the existing methods, the proposed method has advantages in both prediction accuracy and robustness.

Keywords
remaining useful life, aero-engine, adaptive prediction

1. Introduction

As a key component of an aircraft, the performance of an aero-engine directly affects the working condition and safety of the aircraft. The structure and working environment of aero-engine are relatively complicated, and it is very prone to performance degradation and flight failure [1]. To reduce the safety risk and economic loss, aero-engine should adopt the Prognostics and Health Management (PHM) technology to improve the stability and reliability [2]. As one of the core steps in PHM technology, RUL prediction is of great significance in developing maintenance strategies, extending service life and ensuring flight safety. Through accurate RUL prediction, maintenance can be arranged more scientifically to maximize the performance potential.

The prediction methods of RUL are mainly divided into physical model-based and data-driven prediction methods [3]. The first method is to build the corresponding model according to the failure mechanism and structural characteristics, and the quality of the physical model directly affects the prediction effect. However, because of the high precision and complexity of aero-engine, the accurate physical models are difficult to be constructed, resulting in relatively low prediction accuracy. Therefore, the development space of this method is relatively

(*) Corresponding author.
E-mail addresses: X. Liu (ORCID: 0009-0007-5996-6909) a1323061826@163.com, C. Sun (ORCID: 0009-0009-5642-0227) c617391126@163.com
T. Li (ORCID: 0009-0002-9312-3845) a1393434929@163.com

limited. In comparison, the second method extracts and learns the feature information, and constructs the relationship between the features and RUL, which can achieve accurate RUL prediction without complex physical modelling. Therefore, this method has become one of the most effective methods of RUL prediction.

Literature [4] introduces a location-sensitive self-attention unit, which enhances the perception of local context by focusing on the location relationship of the input data, and employs a kind of memory network for the RUL prediction of the potential features on different time scales. Literature [5] proposes a new RUL prediction method for aero-engine based on multi-scale feature extractor, and the transformer model is adopted to further capture features. Finally, the effectiveness of this method is verified through experiments. Literature [6] proposes an interpretable prediction method under complex operating conditions, and the effectiveness and superiority are proved through experiments. To improve the prediction accuracy in complex scenarios, Literature [7] adopts a prediction model in a dual-path framework to enhance the capture ability, and proposes a fusion mechanism to overcome the overfitting and computationally intensive problems of the deep complex model. Literature [8] designs an attention mechanism to extract feature information, and the method is demonstrated to significantly outperform other models in RUL prediction. Literature [9] uses multi-sensors to simulate datasets under four different operating environments and failure mechanisms, and investigates the effects of different models in RUL prediction, as well as their capabilities and limitations. Literature [10] proposes a prediction method based on CNN-LSTM-Attention model, which is experimentally demonstrated to have high accuracy and reliability. Literature [11] obtains high RUL prediction accuracy by optimizing the parameter selection and verifies the advantages of the method with C-MAPSS dataset. Literature [12] adopts a model structure aiming at effective RUL prediction, and proposes the dynamic prediction maintenance strategy. Finally, the experiments indicates that this strategy has good performance compared with the existing maintenance strategies. Literature [13] proposes a new RUL prediction framework to fully utilize the deep feature information in the original data. The experiments indicates that this method has good prediction performance. Literature [14] proposes Neural Ordinary Differential Equations (NODEs) for machinery prognostics tasks, which use neural networks to define differential equations. And the performance of different networks is compared by using C-MAPSS dataset. The results shows that NODEs can compete with state-of-the-art machinery prognostics methods. To address the RUL prediction problem, literature [15] proposes a Deep Equilibrium Model (DEM) that effectively captures sensor information by combining convolutional layers and a novel dual-input interconnection mechanism, and enhances regularization and performance by using Monte Carlo Dropout (MCD) technique. Experimental results show that the proposed method can significantly improve the RUL prediction accuracy.

The above-mentioned methods adopt a uniform initial value and change rule the RUL labelling for aero-engines, which do not fully take into account the influence of the individual differences among different engines on the degradation process. And the original degradation curve is often over-smoothed, losing some intrinsic degradation information, which makes the RUL labels of the original data inaccurate and seriously affects the prediction. Meanwhile, the flight parameters are highly coupled time-series data, and it is difficult for the current method to extract the temporal features and long-term dependencies, which leads to the low prediction accuracy. To realize accurate RUL prediction, an adaptive prediction method for individual differences of engines is proposed. Firstly, PCA algorithm is adopted to lower the dimensionality of the original data, and the filtering method based on wavelet transform is utilized to remove the noise interference. Then, the position of the FPT is determined by calculating the maximum volatility value of the HI curve, so as to obtain the accurate RUL label. On this basis, the improved TCN model is used to capture both local degradation patterns and global features. Then enter the bidirectional cyclic network to model the temporal features in the forward and backward directions, so as to further enhance the extraction of feature information. Finally, the gradual dimensionality reduction is carried out by the deep regression network, and the predicted RUL values are obtained by a single neuron output layer, thereby achieving the end-to-end mapping from multi-source features to RUL values. In the aero-engine RUL prediction experiments, RMSE and MAE of the proposed method are as low as 12.65 and 10.73. The contributions are

summarized as follows:

(1) The adaptive RUL labelling method based on HI and FPT is adopted to obtain accurate labels for the original dataset, which fully takes into account the influence of the individual differences among different engines on the degradation process.

(2) The aero-engine RUL prediction model based on TBiLGF-Net is proposed. This model can accurately predict the RUL of different engines and has good generalization.

(3) Compared with other methods, the proposed method has better accuracy and robustness with only a small increase in computing time, which provides a significant performance advantage.

The rest is as follows. Section 2 illustrates the adaptive RUL labelling method. Section 3 details the TBiLGF-Net model. Section 4 analyses the experimental results under different conditions. Finally, the findings are summarized in Section 5.

2. Adaptive RUL labelling method

To solve the problems of the existing methods mentioned above, an adaptive RUL labelling method based on HI and FPT is adopted. According to previous studies [16-17], the operation of an aero-engine is divided into normal and degradation phases, and usually enters the degradation phase in the range of 35%-55% of the whole cycle period [18]. The whole aero-engine RUL decay process can be represented by a piecewise linear model. According to the Fig. 1, in the initial stage, the engine operates normally. Under the assumption of no degradation, the RUL value of the engine remains constant. When the FPT point is reached, the engine begins to deteriorate. At this point, the RUL value gradually decreases linearly until the engine fails. The whole flow of the adaptive RUL labelling method is shown in Fig. 2.

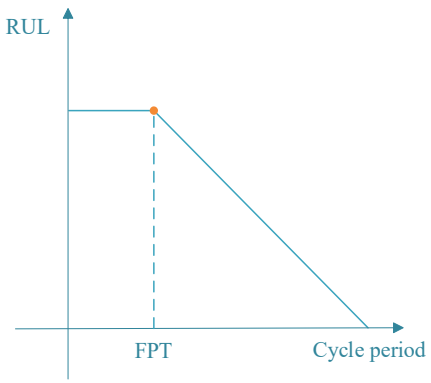

Fig. 1. Piecewise linear model of RUL.

(1) The PCA algorithm is adopted to lower the dimensionality of the original data, and simplify the multidimensional temporal data into one-dimensional degenerate curve, retaining only the first principal component. This approach is sufficient to retain the main degradation information to label RUL and can avoid the introduction of redundant noise [19], so as to clearly reflect the degradation of performance over time.

(2) The filtering method based on wavelet transform is utilized to remove the noise interference of the one-dimensional degradation curve, where the basis function is the Daubechies 4-tap wavelet. This method can effectively suppress the noise while better preserving the local key features in the degradation process, thus obtaining a more realistic HI curve [20]. The filtering method mainly includes the following steps:

1) Wavelet Transform:

$$cA_j[k] = \sum_n h[n-2k] \cdot cA_{j-1}[n] \tag{1}$$

$$cD_j[k] = \sum_n g[n-2k] \cdot cA_{j-1}[n] \tag{2}$$

where $cA_j[k]$ and $cD_j[k]$ are the approximation coefficients and detail coefficients; $h[n]$ and $g[n]$ are respectively the coefficients of the low-pass filter and high-pass filter; k is the discrete-time indexes; and n is the summation indexes.

2) Thresholding:

$$T = \sigma\sqrt{2\ln N} \tag{3}$$

where T is the set threshold; σ is the standard deviation of the highest frequency subband coefficient; $N$is the length of the signal.

$$\widehat{c_{-}}_j[k] = \begin{cases} cD_j[k], |cD_j[k]| \geq T \\ 0, |cD_j[k]| < T \end{cases} \tag{4}$$

3) Wavelet inversion:

$$cA_{j-1}[n] = \sum_k \tilde{h}[n-2k] \cdot cA_j[k] + \sum_k \tilde{g}[n-2k] \cdot cD_j[k] \tag{5}$$

Where $\tilde{h}[n]$ and $\tilde{g}[n]$ are the coefficients of the low-pass and high-pass reconstruction filter.

(3) Calculate the volatility of the HI curve within the range of 35%-55% of the whole cycle, and take the cycle period corresponding to the maximum value as the FPT point position, and determine the RUL value of the current cycle period in combination with the maximum cycle period of the engine. By dynamically calculating the volatility, the degradation starting

point can be determined according to the difference among different engines, avoiding the misjudgement caused by using a fixed threshold and making the labelling of RUL more accurate. The volatility of HI and the formula for calculating RUL are respectively:

$$V_i = \left|\frac{hi_{i+2}+hi_i-2hi_{i+1}}{(t_{i+1}-t_i)^2}\right| \tag{6}$$

where V_i is the HI volatility, hi_i and t_i are respectively the HI value and period of the $i-th$ data.

$$\text{RUL} = \begin{cases} P - FPT, N \leq \text{FPT} \\ P - N, N > \text{FPT} \end{cases} \tag{7}$$

Where P is the maximum cycle period; N is the current cycle period.

Under the premise of better retaining the degradation information, the degradation features are effectively enhanced to accurately identify the position of the FPT point in the HI curve, thereby achieving the adaptive labelling of RUL. This method can fully consider the individual differences among various engines compared with other methods, thus obtaining more realistic RUL labels.

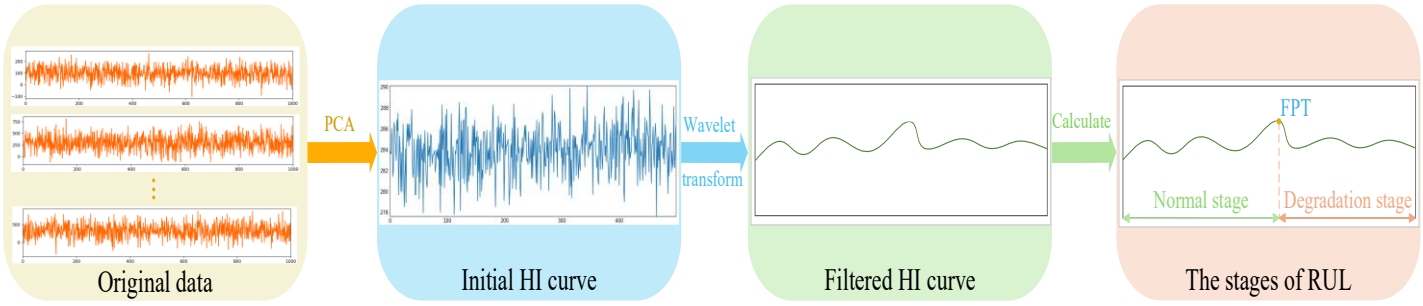

Fig. 2. Flow diagram of adaptive RUL labelling method.

3. TBiLGF-Net

The TBiLGF-Net model is constructed based on TCN, BiLSTM and BiGRU, and combines the BatchNorm layer, LeakyReLU layer, Dropout layer, Pooling layer, Residual Networks, and Fully Connected layer together.

3.1. TCN

Based on the basic framework of CNN, the TCN model can effectively capture sequence dependencies through the integration of causal convolution, dilated convolution and residual connection [21]. The structure is shown as Fig. 3.

When processing a time series $\{x_0, x_1, \ldots, x_T\}$, TCN generates the corresponding output sequence $\{\hat{y}_0, \hat{y}_1, \ldots, \hat{y}_T\}$ by means of a causal convolutional constraint mechanism, which ensures that the output relies only on historical information. The related functions are mapped as follows:

$$\hat{y}_0, \hat{y}_1, \ldots, \hat{y}_T = f(x_0, x_1, \ldots, x_T) \tag{8}$$

In order to break through the local perception limitation of traditional convolution, the dilated convolution technology is adopted in the TCN model, which can significantly extend the receptive field and effectively integrate context information while maintaining the computational efficiency. For a given filter $f: \{0,1,\ldots,k-1\} \to R$, the dilated convolution is defined as:

$$F(s) = (x_d^* f)(s) = \sum_{k-1}^{i=0} f(i) \cdot x_{s-d_i} \tag{9}$$

where k is the filter size; d is the dilation factor; * is the convolution operator.

At the feature extraction level, TCN adopts a modular residual structure, where each residual unit contains a weight normalization layer, a Dropout layer and a Relu activation layer. This hierarchical design realizes cross-layer feature transfer through residual connections, which can solve the gradient decay problem, and improve the ability to capture feature. Compared with the CNN model, TCN can capture the long-range dependencies more efficiently, and effectively fuses the multi-scale historical information. Consequently, TCN is appropriate for complex temporal data containing multiple coupled features, such as the gas path parameters in this paper.

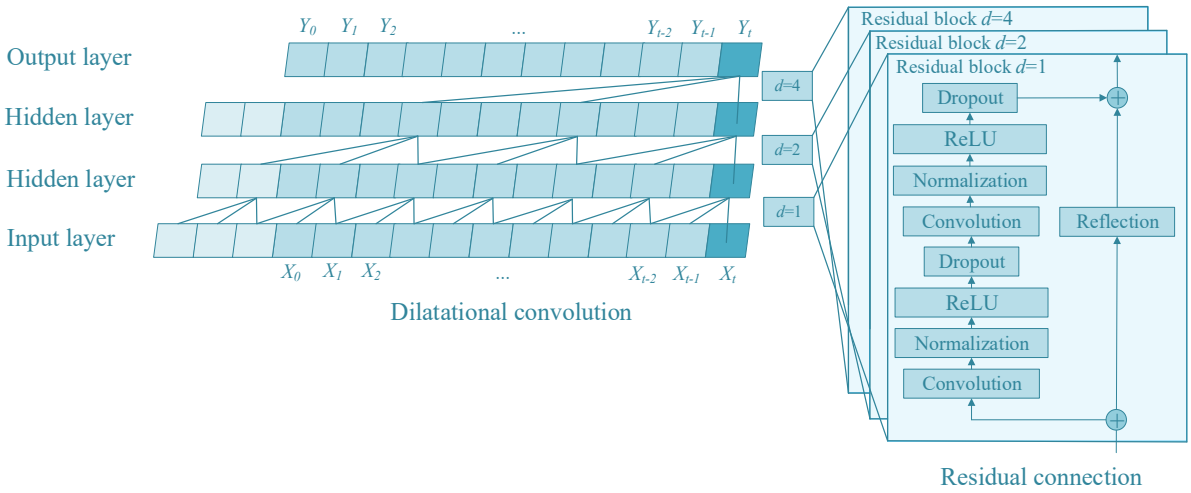

Fig. 3. Structure diagram of TCN model.

3.2. BiLSTM

LSTM model breaks through the limitations of RNN by introducing the gating mechanism, and successfully solves the difficulties of gradient vanishing and processing long sequences [22], as shown in Fig. 4. The LSTM model is composed of an input gate, a forgetting gate and an output gate, in which the input gates are responsible for controlling the entry of data, the forgetting gates regulate the retention degree of the historical data, and the output gates control the output of the final data. This design effectively mitigates the problem of gradient vanishing and can capture long-term patterns. Meanwhile, LSTM model can resolve multi-scale temporal features layer by layer by stacking the memory units in layers, and significantly improves the computational efficiency by using parallelized computation, which is more suitable for dealing with aero-engine gas path parameters with non-stationary characteristics.

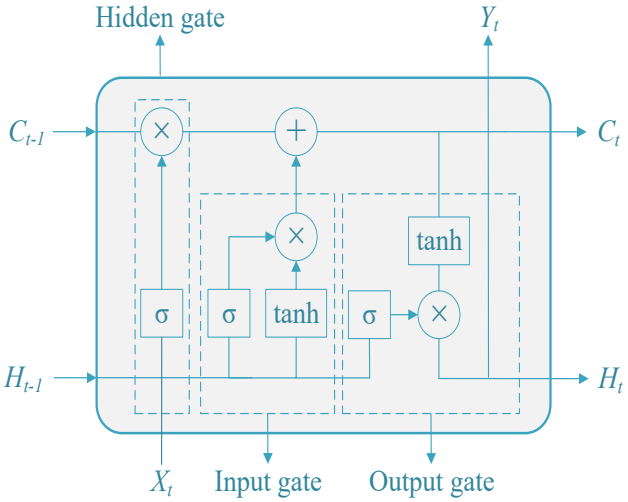

Fig. 4. Structure diagram of LSTM model.

(1) The output of an input gate, a forget gate and an output gate are as follows:

$$I_t = \sigma(W_i * [H_{t-1}, X_t] + B_i) \quad (10)$$

$$F_t = \sigma(W_f * [H_{t-1}, X_t] + B_f) \quad (11)$$

$$Y_t = \sigma(W_y * [H_{t-1}, X_t] + B_y) \quad (12)$$

where X_t is the input vector; H_{t-1} is the hidden state; W_i, W_f and W_y are the weight matrix of the three gates; B_i, B_f and B_y are the bias of the three gates.

(2) The candidate state G_t and the updated state C_t are respectively:

$$G_t = tanh(W_g * [H_{t-1}, X_t] + B_g) \quad (13)$$

$$C_t = F_t * C_{t-1} + I_t * G_t \quad (14)$$

where C_{t-1} is the previous moment memory cell state.

(3) The hidden state H_t:

$$H_t = Y_t * tanh(C_t) \quad (15)$$

The BiLSTM is composed of a forward LSTM layer and a backward LSTM layer, as shown in Fig. 5. These two parts process the input sequence in the forward and reverse orders respectively, which can consider the information before and after the current moment simultaneously. Compared with traditional unidirectional LSTM, BiLSTM models provide richer and more comprehensive contextual information and realize the fusion of past and future information [23]. Therefore, BiLSTM model is more suitable for handling the gas path parameters in this paper.

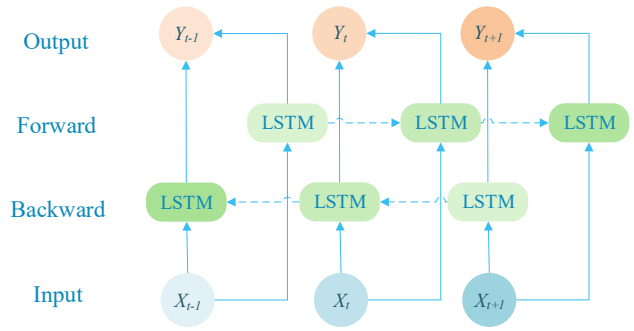

Fig. 5. Structure diagram of BiLSTM model.

3.3. BiGRU

As an improved form of RNN, GRU not only effectively alleviates the common gradient vanishing problem in traditional RNN, but also has a simple structure and high computational efficiency. The GRU is suitable for extracting short-term dependencies in the original data, as shown in Fig. 6.

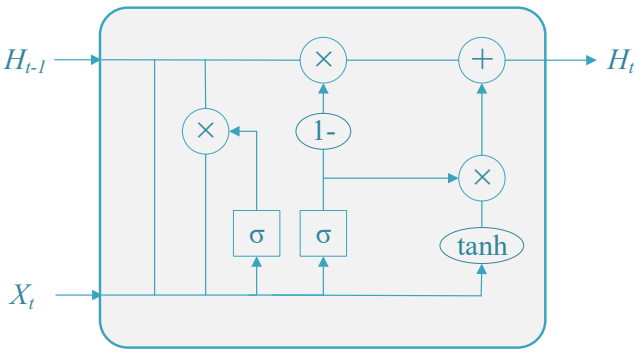

Fig. 6. Structure diagram of GRU model.

The GRU is composed of a reset gate and an update gate [24]. The calculation formulas are as follows:

（1）Reset Gate：

$$R_t = \sigma(W_r \cdot [H_{t-1}, X_t] + B_r) \tag{16}$$

where X_t is the input vector; W_r is the weight matrix; B_r is the bias.

（2）Update Gate：

$$Z_t = \sigma(W_z \cdot [H_{t-1}, X_t] + B_z) \tag{17}$$

（3）Candidate State：

$$\widetilde{H}_t = tanh(W_h \cdot [R_t \odot H_{t-1}, X_t] + B_h) \tag{18}$$

（4）Hidden state：

$$H_t = (1 - Z_t) \odot H_{t-1} + Z_t \odot \widetilde{H}_t \tag{19}$$

In the original unidirectional GRU structure, the information about the current moment depends only on the past time series. However, in many time series tasks, not only the past sequences have an impact on the current moment, but also the future sequences can provide important feedback information. Based on this concept, the BiGRU model is introduced, as shown in Fig. 7. The core idea of BiGRU is to simultaneously analyse the forward and reverse input sequences and fuse the two outputs. This can capture the contextual information more effectively, and provide a more comprehensive and accurate feature representation [25]. BiGRU quickly extracts short-term temporal data features through a lightweight bi-directional GRU. After the combination of BiGRU and BiLSTM, the model can cover more features of different time scales, thereby effectively improving robustness and computational efficiency.

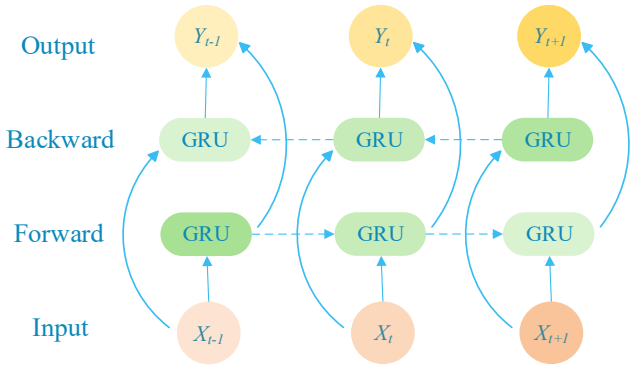

Fig. 7. Structure diagram of BiGRU model.

3.4. Overall structure

The TBiLGF-Net model includes TCN, bidirectional cyclic network and deep regression network, and all the layers are followed by BatchNorm, LeakyReLU and Dropout layers to inhibit the overfitting and improve robustness [26]. The structure is shown in Fig. 8.

The TCN contains five convolution layers, and the dilation rate of each convolution is respectively 1, 2, 4, 8, and 16, gradually expanding the sensory field to capture local details with long-term dependencies. Meanwhile, residual connections are introduced to convey the original input information, effectively alleviating the gradient vanishing problem of the deep network [27]. The bidirectional cyclic network adopts a synergistic architecture of BiLSTM and BiGRU to model the long and short-term temporal features from both the forward and reverse directions respectively. Then another BiLSTM layer is adopted to aggregate the global temporal information. Meanwhile, global maximum pooling and global average pooling are introduced to extract local and global features [28], and the results are fused with the output of BiLSTM layer to form comprehensive degradation features. The deep regression network is composed of fully connected layers of different dimensions and residual connections are added to optimize the

gradient flow. The comprehensive degradation features are dimensionally reduced through each fully connected layer. Finally, the single neuron output layer is utilized to obtain the RUL value, which realizes the end-to-end mapping from multi-source features to RUL value.

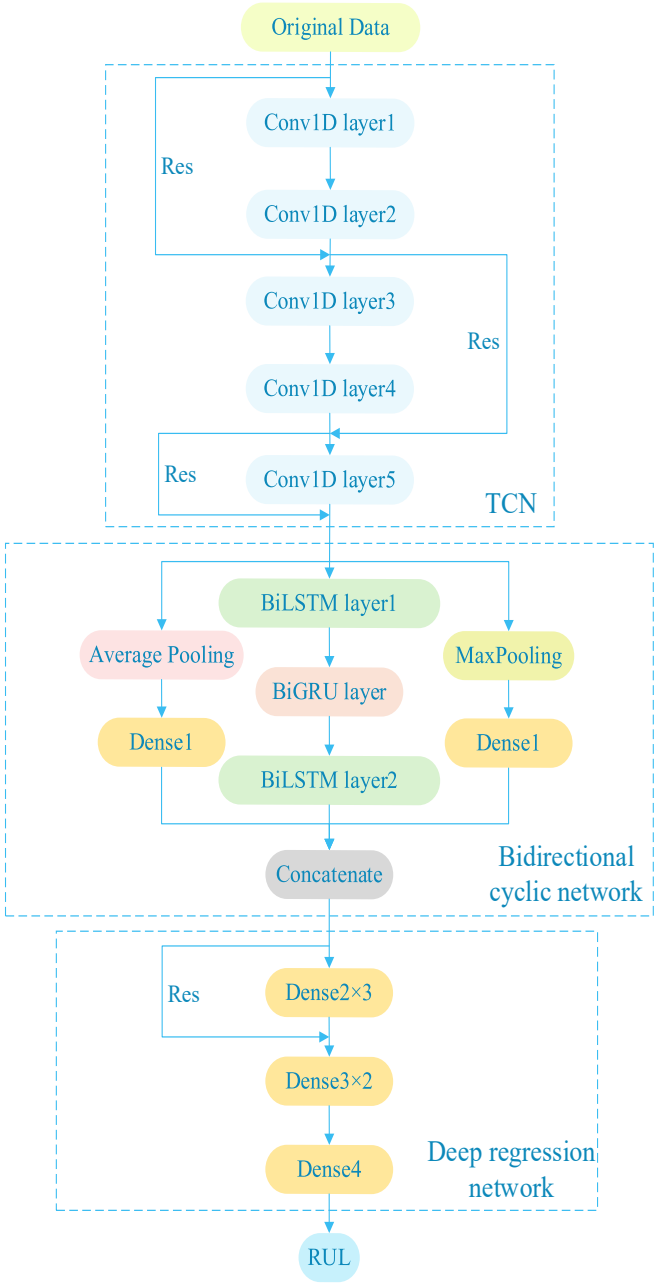

Fig. 8. Structure diagram of TBiLGF-Net model.

The model systematically solves the challenges of temporal features extraction and degradation modelling through multi-scale sensing by dilated convolution, temporal modelling by bidirectional cyclic network, feature fusion by global pooling branching, and cross-layer optimization by residual connect, which enables accurate RUL prediction.

4. Experimental results and analysis

4.1. Experimental dataset

The aero-engine RUL prediction experiments use the C-MAPSS dataset, as shown in Table 1. The dataset records the 24-dimensional data obtained from multiple aero-engines, of which the first three dimensions represent the operating conditions of the engines, and the remaining 21 dimensions represent the values of the engine performance parameters. In this paper, only the 21-dimensional performance parameters are used for the experiments. Specially, all samples in the training set have no corresponding RUL label, and only the last sample of each engine in the test set has the corresponding RUL label.

Table 1. C-MAPSS dataset.

Dataset	FD001	FD003
Number of engines in the training set	100	100
Number of engines in the test set	100	100
Type of working condition	1	1
Fault type	1	2

Before the experiment, it is necessary to adopt the normalization method to eliminate the influence among different feature dimensions. The formula is as follows [29]:

$$\overline{X_t} = \frac{X_t - X_{min}}{Xmin_{max}} \tag{20}$$

4.2. Assessment index

To measure the prediction effect and compare with other models more intuitively, the commonly used RMSE, MAE and computation time are selected as the assessment indexes. The formulas are as follows:

$$\text{RMSE} = \sqrt{\frac{1}{n}\sum_{i=1}^{n}(\hat{y}_i - y_i)^2} \tag{21}$$

$$\text{MAE} = \frac{1}{n}\sum_{i=1}^{n}|\hat{y}_i - y_i| \tag{22}$$

where $\hat{y}_i$ and y_i are respectively the predicted and actual values.

4.3. Experimental environment

The experiments are conducted using Python 3.8, and the platform software configuration is Pytorch 2.4.1, CUDA 11.7, and CUDNN 8.5. To eliminate the accidental errors, all experiments are repeated independently for 10 times and the average of the results is calculated. The hyperparameters are

shown as Table 2.

Table 2. Hyperparameters of the proposed model.

Hyperparameter	Value
Input size	(1,21)
n_conv_layers	5
Dilation Rate	1,2,4,8,16
kernel_size	3
n_BiLSTM_layers	2
n_GRU_layers	1
Batch_size	64
Learning Rate	0.001
Dropout_rate	0.1

4.4. RUL labelling results

To conduct the experimental study, the adaptive RUL labelling method based on HI and FPT is adopted to label the original data, and selects engine No.5 and engine No.73 in FD001 and FD003 training sets respectively as case studies.

(1) The dimensionality reduction of complex original data is processed by PCA algorithm, and a one-dimensional HI curve containing comprehensive degradation trend is obtained. From the Fig. 9, with the engine cycle period increases, the HI value exhibits a gradual upward trend, accompanied by obvious irregular fluctuations. This is mainly caused by sensor noise, changes in operating conditions and the self-repair phenomenon of the system.

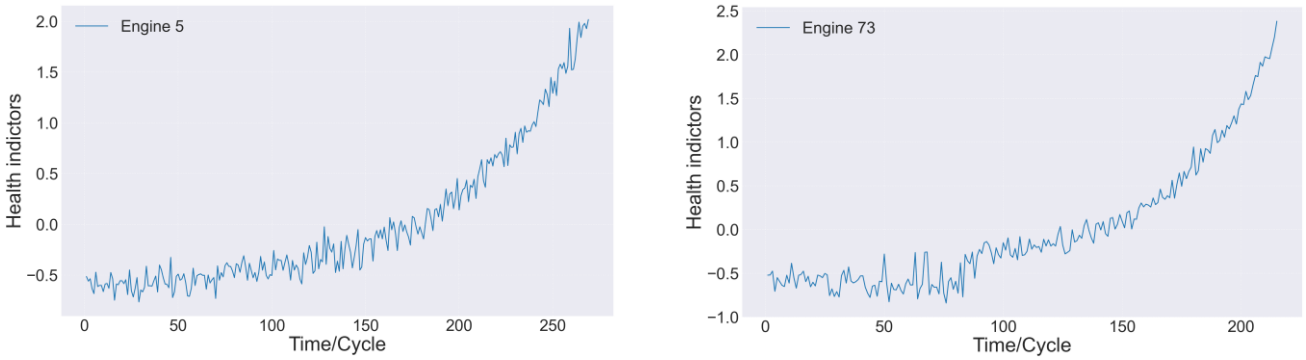

(a) Engine 5 (b) Engine 73

Fig. 9. Initial HI curve of different engines.

(2) The filtering method based on wavelet transform is used to process the HI curve to remove noise interference from the data. Compared with the Fig. 9, the irregular fluctuations of the filtered HI curve in the Fig. 10 are significantly reduced and the trend is more obvious. This indicates that the method can significantly remove high-frequency noise and better retain local degradation characteristics, so that the HI curve reflects a more realistic degradation situation, which is helpful to the accurate identification of FPT points.

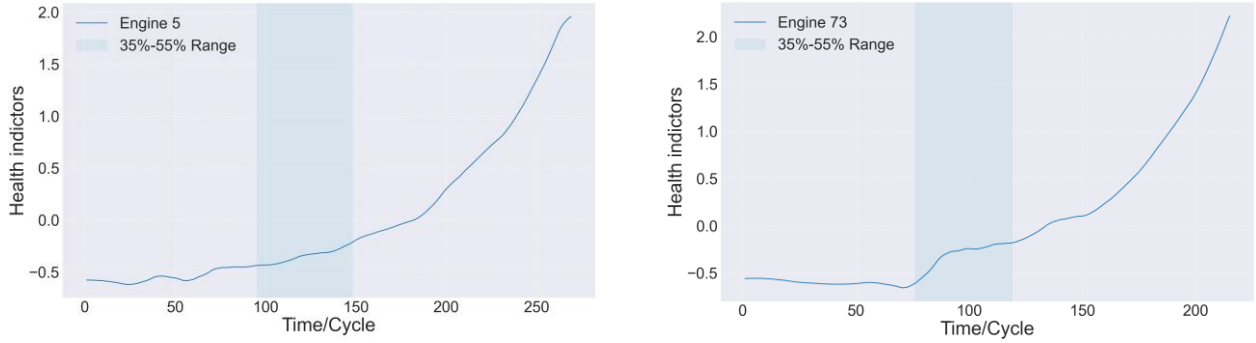

(a) Engine 5 (b) Engine 73

Fig. 10. Filtered HI curve of different engines.

(3) Calculate the volatility of the HI curve in the range of 35%-55% of the whole cycle period, and take the cycle period corresponding to maximum value as FPT point position. According to the Fig. 11, the volatility of the HI curve changes drastically with the increase of the cycle period. This indicates that the engine will have different degrees of degradation phenomena in different operation periods, and the degradation patterns of different engines vary greatly. Therefore, it is necessary to determine the degradation starting point according to the individual differences among different engines in order to

obtain a more accurate RUL value.

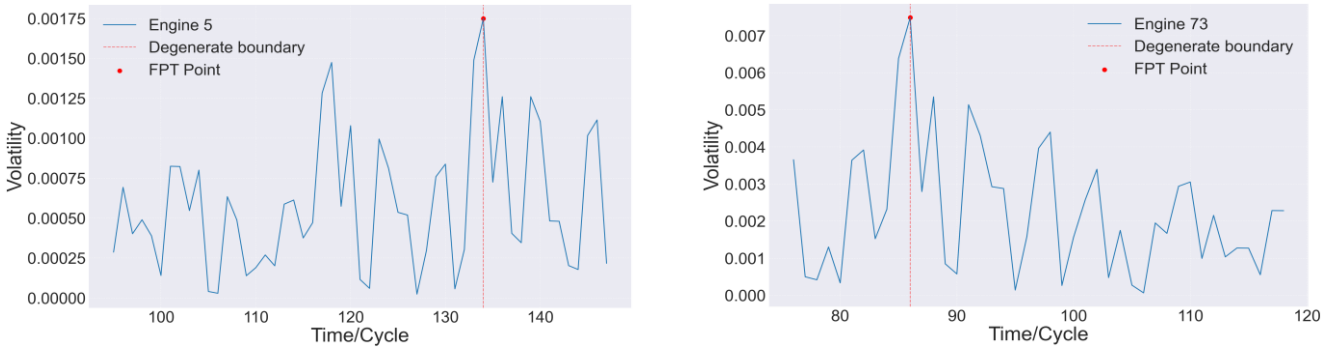

(a) Engine 5 (b) Engine 73

Fig. 11. Volatility curve of different engines.

(4) Determine the RUL value for each engine throughout the entire operation period According to Eq. (7), where the maximum cycle period is the sum of the last cycle period number of each engine and the corresponding RUL value. According to the Fig. 12, RUL remains unchanged in the normal stage and there is no degradation. As the cycle period increases, the engine enters the degradation stage from the normal stage at the FPT point. The RUL value decreases linearly until the engine fails.

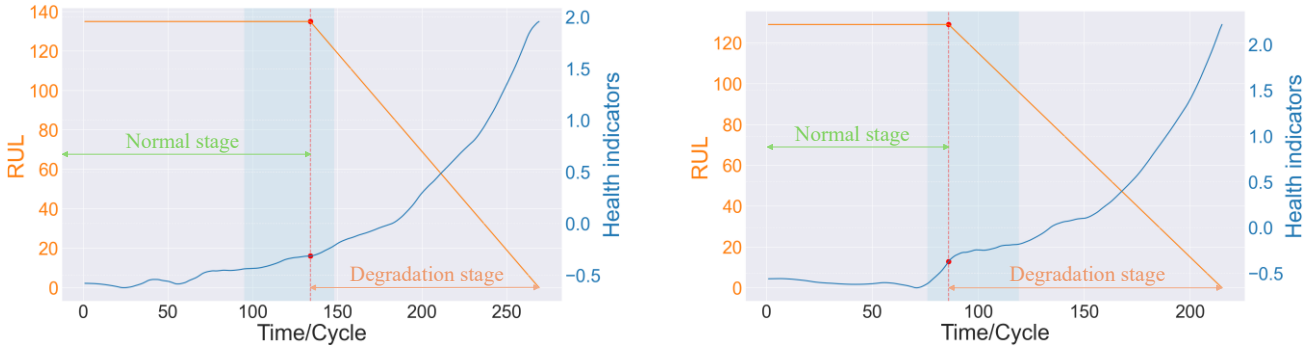

(a) Engine 5 (b) Engine 73

Fig. 12. RUL change curve of different engines.

According to the above process, all the engines in the FD001 and FD003 datasets are labelled to obtain the RUL values and FPT point locations, and the mean and variance are calculated respectively. As can be seen from the Table 3, the mean of the RUL and FPT of each dataset are relatively close to each other, but the variances are quite different, which indicates that the RUL values and degradation start point locations of different engines in the same dataset vary significantly. Moreover, this fully proves that the proposed method can well adapt to the individual differences of different engines, and adapt an exclusive and accurate degradation process for each engine, which has good generalization.

Table 3. RUL labelling results for different datasets.

Dataset	RUL		FPT	
	Mean	Variance	Mean	Variance
FD001 Training set	125.32	75.97	92.59	342.63
FD001 Test set	117.15	102.60	85.65	403.51
FD003 Training set	129.46	121.13	90.29	195.94
FD003 Test set	120.51	97.74	93.82	612.07

4.5. RUL prediction results

To verify the validity of the proposed method, engines No.17 and No.61 in the FD001 test set and No.21 and No.76 in the FD003 test set are selected as test objects for the study. The adaptive RUL labelling method is first adopted to obtain the RUL variation curve of each engine, and then the TBiLGF-Net

model is used to make predictions. According to the Fig. 13, the prediction values of each engine fluctuate relatively stably in the normal stage, and the difference with the true value is within 20 cycles. After entering the degradation stage, the prediction values of each engine start to oscillate and decrease, and the absolute prediction error increases slightly. But the overall trend is basically consistent with the true value, and only a few data points have absolute prediction errors greater than 20 cycles, maintaining a relatively high level of accuracy. Therefore, the proposed method can accurately predict the RUL value and shows good generalization for individual differences of engines.

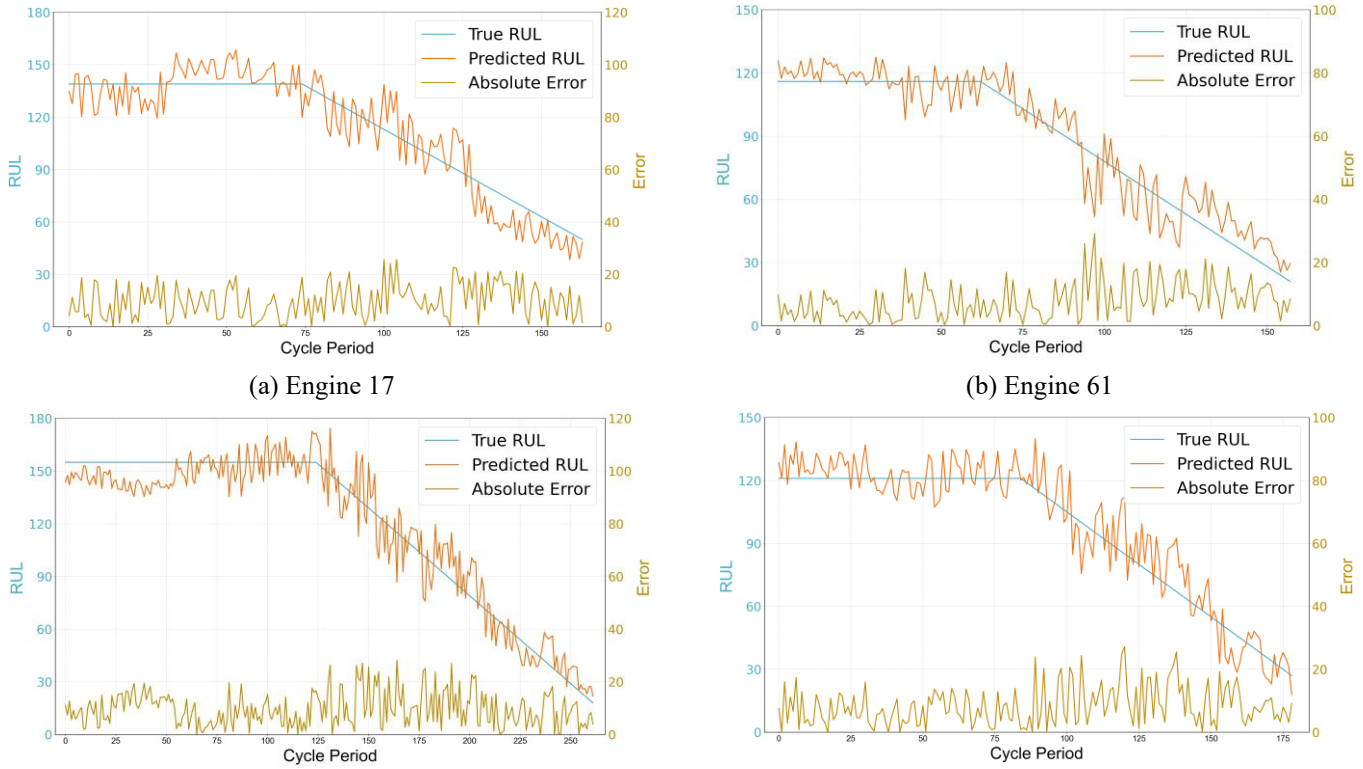

(a) Engine 17 (b) Engine 61

(c) Engine21 (d) Engine 76

Fig. 13. RUL prediction results for individual differences of engines.

4.6. Comparison analysis

To assess the performance, the proposed method is compared with the models of LSTM, CNN-BiLSTM [30], GCN [31], BiGRU-TSAM [32], BNN-HMC [33], DA-LSTM [34], HS-TS [35] and CBHRL [36]. According to the Table 4, the assessment indexes of the proposed method are the lowest values, and the RMSE and MAE can be respectively as low as 12.65 and 10.73. Compared with the other methods, the reduction rates of the RMSE and MAE of the proposed method reaches up to 38.18% and 40.10%, respectively. Even compared with the most accurate of these methods, the reduction rates are up to 5.74% and 6.70%. In addition, in terms of computation time, the proposed method obtains a significant increase in accuracy with a small increase in time consumption compared with the other four most accurate models, achieving a balance between model performance and computational efficiency. Therefore, the model can achieve accurate RUL prediction, and the accuracy is higher than that of other methods, which has a significant advantage.

Table 4. Assessment indexes of different models.

Method	RMSE		MAE		Time(s)	
	FD001	FD003	FD001	FD003	FD001	FD003
LSTM	19.97	20.56	17.85	18.23	39.75	38.63
CNN-BiLSTM	17.12	18.67	16.03	16.45	45.21	49.58
GCN	16.29	16.94	15.59	15.70	41.67	43.05
BiGRU-TSAM	14.21	14.73	12.89	13.06	59.93	62.35
BNN-HMC	13.72	13.96	11.74	11.89	67.70	66.72

Method	RMSE		MAE		Time(s)	
	FD001	FD003	FD001	FD003	FD001	FD003
DA-LSTM	13.70	13.82	11.51	11.63	65.89	67.51
HS-TS	13.59	13.65	11.68	11.77	76.23	75.56
CBHRL	13.42	13.47	11.50	11.59	69.39	70.92
Proposed method	12.65	12.71	10.73	10.92	70.25	71.67

4.7. Ablation experiment

To verify the influence of each component on the overall performance, under the condition of the same hyperparameters, the TBiLGF-Net model is compared with the models of TCN, BiLSTM, BiGRU, TCN-BiLSTM, TCN- BiGRU, BiLSTM-BiGRU.

Table 5. Comparison results of ablation experiment.

Method	RMSE		MAE		Time(s)	
	FD001	FD003	FD001	FD003	FD001	FD003
TCN	18.74	19.36	16.46	17.25	41.35	41.79
BiLSTM	19.62	19.87	17.01	17.29	43.63	45.52
BiGRU	19.87	19.93	17.75	17.82	42.15	43.30
TCN-BiLSTM	14.36	14.72	12.58	12.61	67.07	65.76
TCN-BiGRU	15.46	15.93	13.11	13.38	60.92	61.83
BiLSTM-BiGRU	14.57	14.65	12.27	12.53	66.75	66.41
Proposed method	12.65	12.71	10.73	10.92	70.25	71.67

According to the Table 5, RMSE and MAE of the proposed method are reduced to different degrees compared to the six component models, reaching at least 11.91% and 12.56%. Furthermore, from the perspective of computation time, the increase in the time consumption of the proposed method is relatively small, demonstrating a better cost-performance ratio in terms of performance and efficiency. Therefore, the TCN, BiLSTM and BiGRU models can all significantly improve the prediction accuracy, highlighting the key role of each component of the TBiLGF-Net model in enhancing the prediction performance.

4.8. RUL prediction experiment in noisy environment

In the aero-engine RUL prediction experiments, the experimental results are often affected by noise such as sensor errors and changes in the experimental environment. To verify the performance of different methods under different noise intensities, Gaussian white noise with different signal-to-noise ratios (SNRs) is added to the original data for comparative experiments.

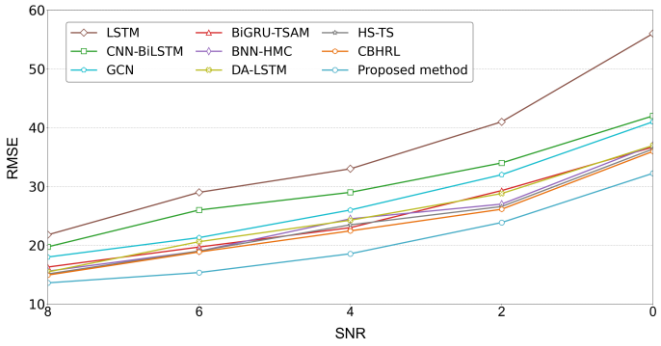

(a) RMSE of FD001

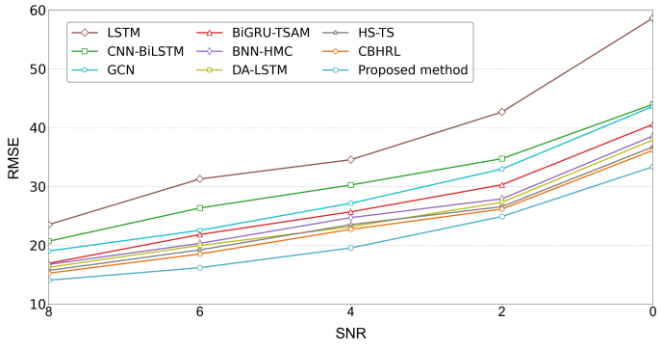

(b) RMSE of FD003

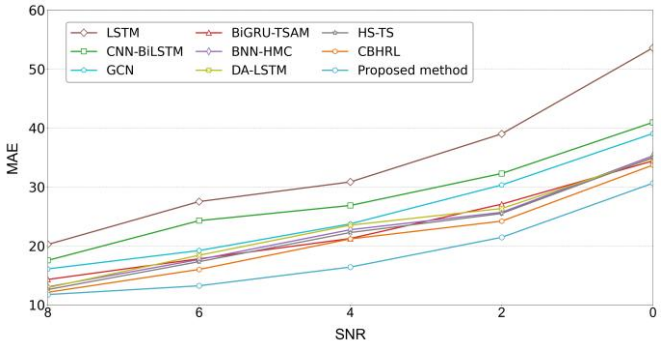

(c) MAE of FD001

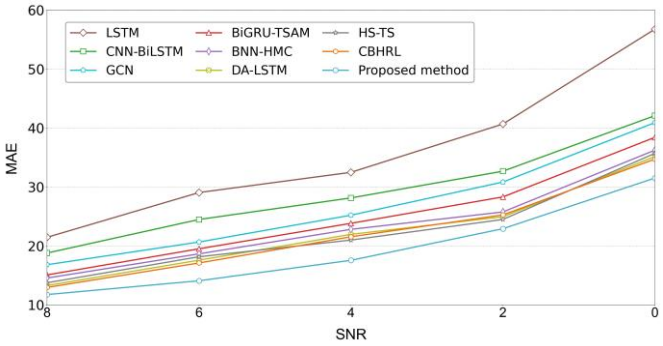

(d) MAE of FD003

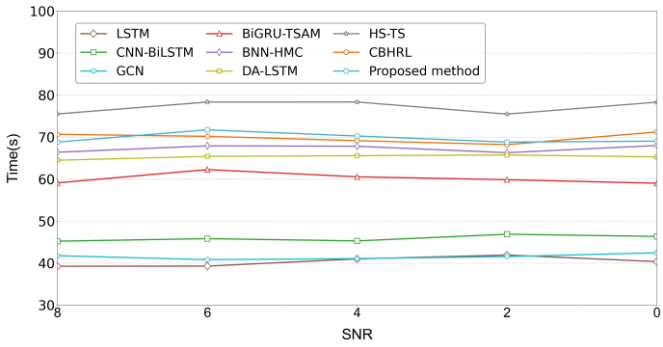

(e) Computation time of FD001

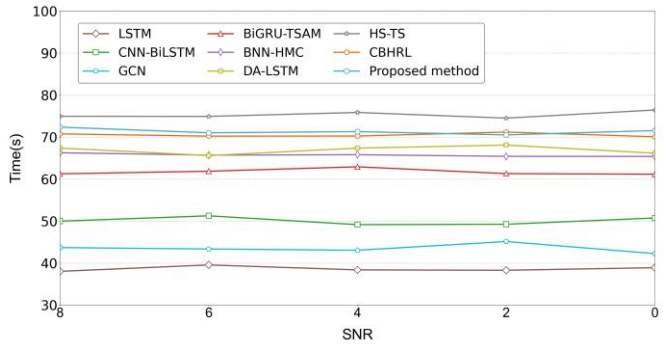

(f) Computation time of FD003

Fig. 14. Assessment indexes of different datasets under different SNRs.

According to the Fig. 14, RMSE and MAE of each method show different degrees of growth as the noise intensity increases, which indicates that the noise will have a certain effect on the accuracy of all models. In the two datasets, RMSE and MAE of the proposed method are the lowest among all the models. Under the extreme noise intensity of SNR0, RMSE and MAE of the proposed method are respectively reduced by at least 7.75% and 9.13% compared with the other methods, and the increase of each assessment index is smallest under different SNRs, which indicates that the proposed model has good robustness. Furthermore, the computing time of each model under different noise intensities is not significantly different, which all fall within the allowable error range. The proposed method achieves a significant improvement in accuracy with only a small increase in computing time, achieving an optimal performance.

5. Conclusion

The existing methods adopt a uniform initial value and change rule the RUL labelling for aero-engines, which do not fully take into account the influence of the individual differences among different engines on the degradation process. And the original degradation curve is often over-smoothed, losing some intrinsic degradation information, which makes the RUL labels of the original data inaccurate and seriously affects the prediction. Meanwhile, the flight parameters are highly coupled time-series data, and it is difficult for the existing method to extract the temporal features and long-term dependencies, which leads to the low prediction accuracy. To realize accurate RUL prediction, an adaptive prediction method for individual differences of engines is proposed. The conclusions are summarized as follows:

(1) The adaptive RUL labelling method based on HI and FPT is adopted to obtain accurate labels for the original dataset, which fully takes into account the influence of the individual differences among different engines on the degradation process. Under the condition of retaining the degradation information well, this method can remove the redundant information and noise interference in the original data, and accurately identify the position of the FPT point in the HI curve, so as to obtain accurate RUL labels.

(2) The prediction model based on TBiLGF-Net is proposed to accurately predict the RUL value of aero-engines. Under different test sets, RMSE and MAE can respectively reach as low as 12.65 and 10.73, demonstrating high prediction accuracy and good generalization across different engines.

(3) Compared with other methods, RMSE and MAE of the

proposed method have decreased by at least 5.74% and 6.70% respectively with only a small increase in computing time, showing higher performance. Under the extreme noise intensity of SNR0, RMSE and MAE of the proposed method are respectively reduced by at least 7.75% and 9.13% than other methods, and the increase of each assessment index is smallest under different SNRs, showing good robustness.

The proposed method has achieved better results for the RUL prediction, but there are still some areas that need to be improved: (1) The structure of the model is relatively complex, which leads to longer calculation time. While ensuring the prediction accuracy, it is necessary to optimize the structure and parameters for improving the operational efficiency and practicality of the model; (2) The proposed method mainly focuses on RUL prediction for aero-engines, and needs to be extended to other more complex application scenarios in the future, so as to satisfy diversified industrial needs.

Acknowledgment

This research did not receive any specific grant from funding agencies in the public, commercial, or not-for-profit sectors. The authors would like to thank the comments from the anonymous reviewers that improved the quality of the paper.

References

1. Zavila O, Hocko M, Buba H, et al. Analysis of aviation accidents associated with aircraft jet engine surge, on-board fire and crew ejection[C]//2019 Modern Safety Technologies in Transportation (MOSATT). IEEE, 2019: 152-155. https://doi.org/10.1109/MOSATT48908.2019.8944108
2. Omshi E M, Grall A. Replacement and imperfect repair of deteriorating system: Study of a CBM policy and impact of repair efficiency[J]. Reliability Engineering & System Safety, 2021, 215: 107905.
3. Chen Z, Wu M, Zhao R, et al. Machine remaining useful life prediction via an attention-based deep learning approach[J]. IEEE Transactions on Industrial Electronics, 2020, 68(3): 2521-2531. https://doi.org/10.1109/TIE.2020.2972443
4. Chen X. A novel transformer-based DL model enhanced by position-sensitive attention and gated hierarchical LSTM for aero-engine RUL prediction[J]. Scientific Reports, 2024, 14(1): 10061. https://doi.org/10.1038/s41598-024-59095-3
5. Guo J, Lei S, Du B. MHT: A multiscale hourglass-transformer for remaining useful life prediction of aero-engine[J]. Engineering Applications of Artificial Intelligence, 2024, 128: 107519.
6. Gao J, Wang Y, Sun Z. An interpretable RUL prediction method of aero-engine under complex operating conditions using spatio-temporal features[J]. Measurement Science and Technology, 2024, 35(7): 076003. https://doi.org/10.1088/1361-6501/ad3b2c
7. Lu X, Pan H, Zhang L, et al. A dual path hybrid neural network framework for remaining useful life prediction of aero‐engine[J]. Quality and Reliability Engineering International, 2024, 40(4): 1795-1810. https://doi.org/10.1002/qre.3494
8. Fan Z, Li W, Chang K C. A two-stage attention-based hierarchical transformer for turbofan engine remaining useful life prediction[J]. Sensors, 2024, 24(3): 824. https://doi.org/10.3390/s24030824
9. Judeson Antony Kovilpillai J, Mohamed S S, Pragya, et al. Deep Learning Models for Enhanced RUL Prediction in Turbofan Jet Engines[C]//International Conference on Emerging Trends and Technologies on Intelligent Systems. Singapore: Springer Nature Singapore, 2024: 685-699. https://doi.org/10.1007/978-981-97-5703-9_56
10. Deng S, Zhou J. Prediction of remaining useful life of aero-engines based on CNN-LSTM-Attention[J]. International Journal of Computational Intelligence Systems, 2024, 17(1): 232. https://doi.org/10.1007/s44196-024-00639-w
11. Abdelghafar S, Khater A, Wagdy A, et al. Aero-engines remaining useful life prediction based on enhanced adaptive guided differential evolution[J]. Evolutionary Intelligence, 2024, 17(2): 1209-1220. https://doi.org/10.1007/s12065-022-00805-z
12. Wang L, Zhu Z, Zhao X. Dynamic predictive maintenance strategy for system remaining useful life prediction via deep learning ensemble method[J]. Reliability Engineering & System Safety, 2024, 245: 110012.
13. Shang J, Xu D, Qiu H, et al. A novel data augmentation framework for remaining useful life estimation with dense convolutional regression network[J]. Journal of Manufacturing Systems, 2024, 74: 30-40. https://doi.org/10.1016/j.jmsy.2024.02.011
14. Star M, McKee K. Remaining useful life estimation using neural ordinary differential equations[J]. International Journal of Prognostics and Health Management, 2021, 12(2). https://doi.org/10.36001/ijphm.2021.v12i2.2938

15. Plakias S, Boutalis Y S. A Deep Equilibrium Model for Remaining Useful Life Estimation of Aircraft Engines[J]. Electronics, 2025, 14(12): 2355. https://doi.org/10.3390/electronics14122355
16. Zhou L, Wang H, Xu S. Aero-engine prognosis strategy based on multi-scale feature fusion and multi-task parallel learning[J]. Reliability Engineering & System Safety, 2023, 234: 109182.
17. Zhang Y, **n Y, Liu Z, et al. Health status assessment and remaining useful life prediction of aero-engine based on BiGRU and MMoE[J]. Reliability Engineering & System Safety, 2022, 220: 108263.
18. Yan J, He Z, He S. Multitask learning of health state assessment and remaining useful life prediction for sensor-equipped machines[J]. Reliability Engineering & System Safety, 2023, 234: 109141.
19. Pishini K, Abdolazimi O, Shishebori D, et al. Evaluating efficiency in water and sewerage services: An integrated DEA approach with DOE and PCA[J]. Science of The Total Environment, 2025, 959: 178288.
20. Afrasiabi A, Faramarzi A, Chapman D, et al. Optimising Ground Penetrating Radar data interpretation: A hybrid approach with AI-assisted Kalman Filter and Wavelet Transform for detecting and locating buried utilities[J]. Journal of Applied Geophysics, 2025, 232: 105567.
21. Zhang L, Ren G, Li S, et al. A novel soft sensor approach for industrial quality prediction based TCN with spatial and temporal attention[J]. Chemometrics and Intelligent Laboratory Systems, 2025, 257: 105272.
22. Wang L, Zhao W. An ensemble deep learning network based on 2D convolutional neural network and 1D LSTM with self-attention for bearing fault diagnosis[J]. Applied Soft Computing, 2025: 112889.
23. Nisha A V, Rajasekaran M P, Kottaimalai R, et al. Rider Cat Optimized Alzheimer’s Disease and MCI Prediction Using Deep Attention BiLSTM and CRDF[J]. IETE Journal of Research, 2025: 1-15. https://doi.org/10.1080/03772063.2025.2451721
24. He X, Zhao W, Gao Z, et al. Short-term load forecasting by GRU neural network and DDPG algorithm for adaptive optimization of hyperparameters[J]. Electric Power Systems Research, 2025, 238: 111119.
25. Feng Y, Hu X, Hou S, et al. A Novel BiGRU-Attention Model for Predicting Corn Market Prices Based on Multi-Feature Fusion and Grey Wolf Optimization[J]. Agriculture, 2025, 15(5): 469. https://doi.org/10.3390/agriculture15050469
26. Khaled A. BCN: batch channel normalization for image classification[C]//International Conference on Pattern Recognition. Springer, Cham, 2025: 295-308. https://doi.org/10.1007/978-3-031-78195-7_20
27. Li Y, Lei Y, Yang X. Rethinking residual connection in training large-scale spiking neural networks[J]. Neurocomputing, 2025, 616: 128950.
28. Lee W, Ham B, Kim S. Maximizing the Position Embedding for Vision Transformers with Global Average Pooling[J]. arxiv preprint arxiv:2502.02919, 2025.
29. Peng P, Li Y, Guo Z. High-performance remaining useful life prediction for aeroengine based on combining health states and trajectory similarity[J]. Engineering Applications of Artificial Intelligence, 2025, 141: 109799.
30. Zhu Y, Luo Z, Liu X, et al. Leveraging the hybrid CNN-BiLSTM and multi-head self-attention mechanisms for Aero-engine RUL estimation[C]//2024 8th International Conference on Electrical, Mechanical and Computer Engineering (ICEMCE). IEEE, 2024: 1014-1019. https://doi.org/10.1109/ICEMCE64157.2024.10861912
31. Li T, Zhou Z, Li S, et al. The emerging graph neural networks for intelligent fault diagnostics and prognostics: A guideline and a benchmark study[J]. Mechanical Systems and Signal Processing, 2022, 168: 108653.
32. Zhang J, Jiang Y, Wu S, et al. Prediction of remaining useful life based on bidirectional gated recurrent unit with temporal self-attention mechanism[J]. Reliability Engineering & System Safety, 2022, 221: 108297.
33. Benker M, Furtner L, Semm T, et al. Utilizing uncertainty information in remaining useful life estimation via Bayesian neural networks and Hamiltonian Monte Carlo[J]. Journal of Manufacturing Systems, 2021, 61: 799-807. https://doi.org/10.1016/j.jmsy.2020.11.005
34. Shi J, Zhong J, Zhang Y, et al. A dual attention LSTM lightweight model based on exponential smoothing for remaining useful life prediction[J]. Reliability Engineering & System Safety, 2024, 243: 109821.
35. Peng P, Li Y, Guo Z. High-performance remaining useful life prediction for aeroengine based on combining health states and trajectory similarity[J]. Engineering Applications of Artificial Intelligence, 2025, 141: 109799.
36. Zhu Q, Zhou Z, Li Y, et al. Contrastive BiLSTM-enabled health representation learning for remaining useful life prediction[J]. Reliability Engineering & System Safety, 2024, 249: 110210.